



## Original Paper

# Numerical simulation of the electromagnetic torques of PMSM with two-way magneto-mechanical coupling and nonuniform spline clearance in electric submersible pumping wells



Xin-Fu Liu <sup>a, \*</sup>, Chun-Hua Liu <sup>b, \*\*</sup>, Ying Zheng <sup>c</sup>, Ji-Fei Yu <sup>d</sup>, Wei Zhou <sup>d</sup>, Meng-Xiao Wang <sup>d</sup>, Peng Liu <sup>a</sup>, Yi-Fei Zhou <sup>a</sup>

<sup>a</sup> Key Lab of Industrial Fluid Energy Conservation and Pollution Control (Ministry of Education), Qingdao University of Technology, Qingdao, 266520, Shandong, China

<sup>b</sup> College of Mechanical and Electronic Engineering, China University of Petroleum (East China), Qingdao, 266580, Shandong, China

<sup>c</sup> Department of Chemical and Biochemical Engineering, Western University, Ontario, N6A 3K7, Canada

<sup>d</sup> CNOOC Research Institute Ltd., CNOOC, Beijing, 100028, China

## ARTICLE INFO

## Article history:

Received 12 November 2023

Received in revised form

1 September 2024

Accepted 25 September 2024

Available online 26 September 2024

Edited by Jia-Jia Fei and Teng Zhu

## Keywords:

Permanent magnet synchronous motor

Two-way coupling

Magneto-mechanical coupling

Nonuniform spline clearance

Electromagnetic torque

## ABSTRACT

Clearance-fit (side-fit) spline joints are a key component in a permanent magnet synchronous motor (PMSM) in electric submersible pumping wells. The nonuniform spline clearance affects the output performance of a PMSM. A concept for energy conservation is optimized in this study to improve the modeling accuracy of electromagnetic torque. However, most existing computation models are one-way model with a magneto-mechanical simulation. In this study, a more accurate two-way coupling method is presented for simulating the electromagnetic and mechanical characteristics of PMSM. Additionally, importance should be attached to this two-way magneto-mechanical coupling methodology in an actual simulation. The coupled power, electrical and magnetic energy, and electromagnetic torque equations are solved iteratively until convergence for PMSMs with a segmented rotor and a non-segmented rotor. The optimal electromagnetic torque is obtained for different rotor configurations with the change of temperatures and rotational speeds. The results show that the output performance and electromagnetic torque of the PMSM are seriously affected by the effects of two-way magneto-mechanical coupling and nonuniform spline clearance. The proposed two-way coupling model gives more reasonable predictions than other one-way models do, because the power transfer between the electrical and magnetic energy can be modeled more accurately. The self-centralizing performance of clearance-fit splines and the sensitivity to the radial clearance magnitude lead to the reduction of the electromagnetic torque for the PMSM. Additionally, the electromagnetic torques decrease with the enhanced rotor temperatures and rotational speeds. The best rotor temperature and rotational speed are chosen through a comparison of the experimental results, and then the optimal electromagnetic torque is provided to ensure the output performance of the PMSM in electric submersible pumping wells.

© 2024 The Authors. Publishing services by Elsevier B.V. on behalf of KeAi Communications Co. Ltd. This is an open access article under the CC BY-NC-ND license (<http://creativecommons.org/licenses/by-nc-nd/4.0/>).

## 1. Introduction

With the development of oil production and permanent magnet technology, permanent magnet synchronous motor technology has

advanced rapidly (Ahmed and Toliyat, 2007; Zhu et al., 2007; Ji, 2008; Hao et al., 2019; Isildar et al., 2019; Wan et al., 2020; Liu et al., 2023) in electric submersible pumping wells. PMSMs are becoming increasingly popular due to their high efficiency, power density, power factor, and reliability (Morimoto et al., 2001; Cui et al., 2020; Yang et al., 2020). A spline system consisting of the internal spline and an external spline is widely utilized in PMSMs (Cortes et al., 2019; Johnson and Affam, 2019; Ahn et al., 2021; Klemz et al., 2021). Due to assembly and manufacturing errors, nonuniform spline clearance impacts the performance of PMSMs

\* Corresponding author.

\*\* Corresponding author.

E-mail addresses: [upcdoctor@126.com](mailto:upcdoctor@126.com) (X.-F. Liu), [20090053@upc.edu.cn](mailto:20090053@upc.edu.cn) (C.-H. Liu).

(Fang et al., 2021; Qiao et al., 2013; Zhang and Yang, 2022). Therefore, to precisely forecast the electromagnetic and mechanical characteristics of PMSMs in electric submersible pumping wells, it is essential to take into account the impact of spline clearance.

The use of PMSMs in petroleum exploration has increased in the last two decades. Significant efforts have been made to optimize the design and simulation of PMSMs to improve their mechanical characteristics in electric submersible pumping wells. A method of multi physical domain coupling thermal analysis based on control circuit, electromagnetic and thermal was presented. The validity and accuracy of the multi physical domain coupling thermal analysis method were verified. The temperature rise distribution of key components was accurately simulated using the method (Chen et al., 2017). The extracted modes were studied and the associated Finite Element modal analysis was carried out. Preliminary analysis for identifying the core stiffness from its modal characteristics was presented. Based upon the identified parameters rotor-dynamic analysis was performed for critical speed calculation (Singhal et al., 2011). The modal parameters of the whole PMSM were calculated by using the substructure modal synthesis method. The weak links of the motor were found out and the structure optimization was carried out. The modal parameters of the motor were obtained through the frequency domain analysis method, and the FEA result was confirmed by the modal test of the motor (Zhao et al., 2020). A multi-objective optimization algorithm was employed to determine the rotor design parameters which maximized the output torque of the PMSM over three different load conditions (no load, rated load and maximum speed load) (Wang et al., 2022). A design of line start permanent magnet synchronous motor with consequent magnetic pole was proposed. The number of the permanent magnets (PMs) in the proposed structure was 25% less than the PMs utilized in conventional motors, which could potentially decrease the manufacturing expenses, in particular, in larger size motors (Ghoroghchian et al., 2020).

The rotor of an SR-PMSM comprises several segment rotors connected by splines (Wang et al., 2012; Rallabandi and Fernandes, 2014; Fan et al., 2022). The splines of a PMSM typically transfer a load in complicated subsurface environments. Consequently, excessive wear often occurs before the splines reach their expected life, which can result in the occurrence of clearance fits at the spline joints (Ding et al., 2017; Dong et al., 2019; Chen et al., 2022). The spline clearance changes the torsion angle of the rotor and significantly affects the output performance of a PMSM in electric submersible pumping wells.

In this study, a two-way magneto-mechanical coupling method for a PMSM is investigated based on the traditional one-way coupling method. We improve the accuracy of the traditional model and we propose a novel model to calculate the electromagnetic torque of a PMSM in electric submersible pumping wells. To verify the feasibility of this method, different coupled models are used to calculate the electromagnetic torque of a PMSM. The PMSMs are analyzed first using one-way coupling and then using two-way coupling. Then, a comparison between the mechanical characteristics of a permanent magnet synchronous motor with a non-segmented rotor (NSR-PMSM) and a permanent magnet synchronous motor with a segmented rotor (SR-PMSM) is presented based on 3D-FEA under different operating conditions. Finally, the influences of the rotor structure on the mechanical characteristics are further discussed based on the prototype experiment.

## 2. Mathematical model of electromagnetic torque for a PMSM

When a PMSM is running steadily in electric submersible pumping wells, the energy stored in the air gap magnetic field

changes. A small amount of magnetic energy is converted into mechanical energy and drives the rotation of the rotor (Wang et al., 2009; Hasanien, 2010; Gao et al., 2019).

According to the Energy Conservation Law, the following equation represents the electrical energy consumed by the system.

$$dW_e = dW_{\text{mech}} + dW_m = t_e d\theta_r + dW_m \quad (1)$$

where  $dW_{\text{mech}}$  is the energy converted from electrical energy to mechanical energy in J,  $dW_m$  is the energy converted from electrical energy to magnetic energy in J,  $d\theta_r$  is the electrical angle between the  $d$ -axis and the synthesized magnetic field direction of the stator in rad, and  $t_e$  is the electromagnetic torque in N·m.

Some of the electrical energy input (Yang and Zhang, 2008) to the system is converted into magnetic energy (Redinz, 2023) and some is converted into mechanical energy (Duarte et al., 2018) to drive the rotor. Eq. (2) can be used to determine the total power input to the system.

$$dW_e = \frac{\psi_r}{L_r} d\psi_r + i_s d\psi_s \quad (2)$$

where  $i_s$  is the current in the stator winding in A,  $\psi_r$  is the rotor magnetic flux in Wb,  $L_r$  is the self-inductance of the rotor winding in H, and  $\psi_s$  is the stator magnetic flux in Wb.

The amount of total electrical energy converted into magnetic energy can be represented as:

$$dW_m = \frac{\partial W_m}{\partial \theta_r} d\theta_r + \frac{\psi_r}{L_r} d\psi_r + i_s d\psi_s \quad (3)$$

Eqs. (1)–(3) are solved for the electromagnetic torque  $t_e$  of PMSM (Spalek, 2010; Nishino et al., 2017), as follows:

$$t_e d\theta_r = dW_e - dW_m = \frac{\psi_r}{L_r} d\psi_r + i_s d\psi_s - \frac{\psi_r}{L_r} d\psi_r - i_s d\psi_s - \frac{\partial W_m}{\partial \theta_r} d\theta_r = -\frac{\partial W_m}{\partial \theta_r} d\theta_r \quad (4)$$

Disregarding the magnetic reluctance of the iron core, the stored energy of the motor magnetic field (Morimoto et al., 2014; Li et al., 2019) can be expressed by:

$$W_m = \frac{\psi_r^2}{2L_r} + i_s M_{sr} \frac{\psi_r}{L_r} \cos \theta_r + \frac{1}{2} L_s i_s^2 \quad (5)$$

where  $M_{sr}$  is the maximum mutual inductance between the stator and the rotor in H.

The electromagnetic torque  $t_e$  can be derived by substituting Eq. (5) into Eq. (4), as follows:

$$t_e = -\frac{\partial W_m}{\partial \theta_r} = i_s M_{sr} \frac{\psi_r}{L_r} \sin \theta_r \quad (6)$$

The PMSM generates electromagnetic torque to drive the rotor rotation due to the angular mismatch between the stator and rotor magnetic fields (Kim et al., 2005; Lim et al., 2017; Ilka et al., 2018). Spline clearance leads to an angular shift of the rotor and changes the position of permanent magnets on the rotor, resulting in the electromagnetic torque of the motor being affected. The electromagnetic forces exerted on the PMSM rotor with a high aspect ratio tend to deform it, reducing the electromagnetic torque. These factors have an influence on the electromagnetic torque of the PMSM, which is why the decline rate of the electromagnetic torque is calculated (Zhang et al., 2007; Guemes et al., 2011; Hong et al., 2014; Xu et al., 2023). The linear density of the electromagnetic torque  $\rho$  at a distance  $x$  from the drive end can be obtained with the

following equation:

$$\rho = \frac{t_e \sin(\theta_r + p\delta_r(L_r - x - nL_r) - (n - 1)p\delta_s)}{L_r} \quad (7)$$

where  $p$  is the number of pole pairs,  $\delta_r$  is the torsion angle per unit length in rad,  $\delta_s$  is the torsion angle of the spline in rad, and  $L_r$  is the length of the segmented rotor in mm.

Considering the torsional deformation of the shaft leading to torque reduction, the optimized electromagnetic torque  $T_e$  can be determined as follows:

$$T_e = \sum_{n=1}^n \frac{\sin(\theta - (n - 1)p\delta_r L_r / 2 - (n - 1)p\delta_s) \sin(p\delta_r L_r / 2)}{p\delta_r L_r / 2n} t_e \quad (8)$$

Most existing computation models are one-way model with a magneto-mechanical simulation. In this study, a more accurate two-way coupling method is presented for computing and simulating the electromagnetic and mechanical characteristics of PMSM. The coupled power, electrical and magnetic energy, and electromagnetic torque equations are solved iteratively until convergence for the NSR-PMSMs and the SR-PMSMs with a segmented rotor and a non-segmented rotor.

### 3. Comparison of electromagnetic torque according to coupling methods

To evaluate the electromagnetic and mechanical characteristics of two PMSMs in electric submersible pumping wells, we provide three-dimensional models of the SR-PMSM and NSR-PMSM. The external spline is located on the outer surface of the shaft, while the internal spline is located on the inner surface of the hole. There is a clearance fit between adjacent segment rotors. And the nonuniform clearance is located between the external tooth profile of the internal spline and the internal tooth profile of the external spline of a PMSM, as shown in Fig. 1. The variation of spline clearance due to the existence of load fluctuations can be affected by these factors such as the material of motor shaft and the high ambient temperatures, which will make the numerical simulation more complicated. Consequently, the influence of dynamic clearance changes on electromagnetic torque is ignored for the characteristic analysis of PMSM. And the average spline clearance is 250 μm (Liu et al., 2021).

The numerical simulation of two PMSMs including the rotor, the stator core and the permanent magnet is implemented, and the electromagnetic characteristics are obtained from FEA. The main dimensions and parameters of the two PMSMs are set, as

shown in Table 1.

Fig. 2(a) shows the machine topology of the 18-slot and 16-pole PMSM. The PMSM consists of two essential components: the stator core with winding and the rotor embedded with permanent magnets, and the two PMSMs differ in their rotor and mechanical structures (Zhang et al., 2018). It can be seen that both PMSMs possess identical stator structures, which are composed of eighteen cores. The eighteen stator cores are evenly arranged along the rotor. The only difference between these two PMSMs is the rotor structure. The rotor of the SR-PMSM consists of four separate sections on which 16 permanent magnets are embedded (Akpan et al., 2001; Khulief and Al-Naser, 2005; Iwashita et al., 2020). The length of each segmented rotor is equal to that of each segmented stator. The rotor of the NSR-PMSM is a block without segments like a common rotor.

Fig. 2(b) illustrates the design variables of the motor. The comparison between the NSR-PMSM and the SR-PMSM is made based on finite element analysis (Kim, 2001; Freytag et al., 2011). To ensure a fair comparison, the two PMSMs have the same basic dimensions as well as the number of coils per slot, the material, and the connection types of winding.

In this section, we analyze the electromagnetic and mechanical characteristics of the PMSM using one-way coupling and two-way coupling methods and examine the relationship between the coupling methodology and the simulation results.

The strain and torque of PMSM are calculated with the help of solving the magnetic field by Maxwell module and importing the magnetic force acting on the permanent magnet into Transient Structural module for one-way coupling methodology.

The proposed two-way coupling computation model is verified by finite element method by using ANSYS on each cell zone throughout the PMSM rotor. The strain and torque of PMSM are calculated with the help of solving the magnetic field by Maxwell module and importing the magnetic force acting on the permanent magnet into Transient Structural module. And then the shaft strain

**Table 1**  
The main dimensions and parameters of two PMSMs.

Parameters	NSR-PMSM	SR-PMSM
Rated power $P$ , kW	7.5	7.5
Rated voltage $U$ , V	380	380
Number of poles $p$	16	16
Number of slots $Z$	18	18
Rated speed $n$ , rpm	500	500
Rotor length $s$ , mm	2600	(600 + 50) × 4
Number of total turns $N$	100	100

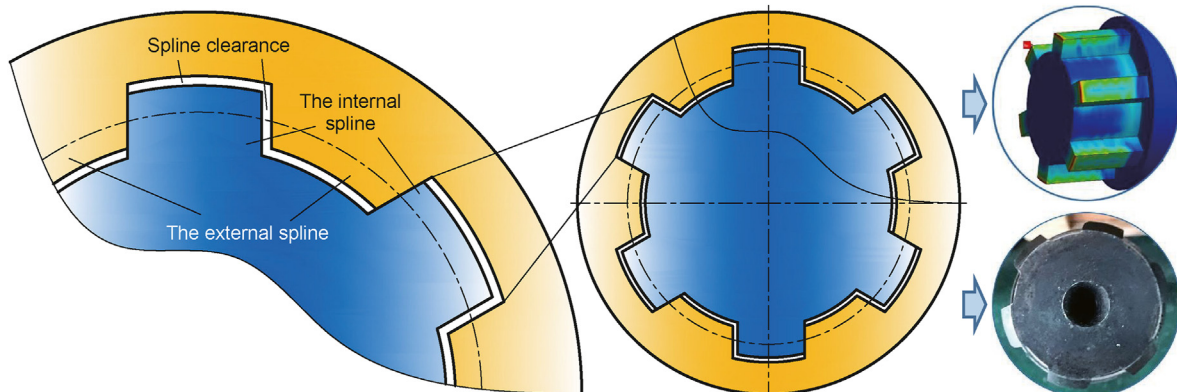


**Fig. 1.** The spline clearance of a permanent magnet synchronous motor.

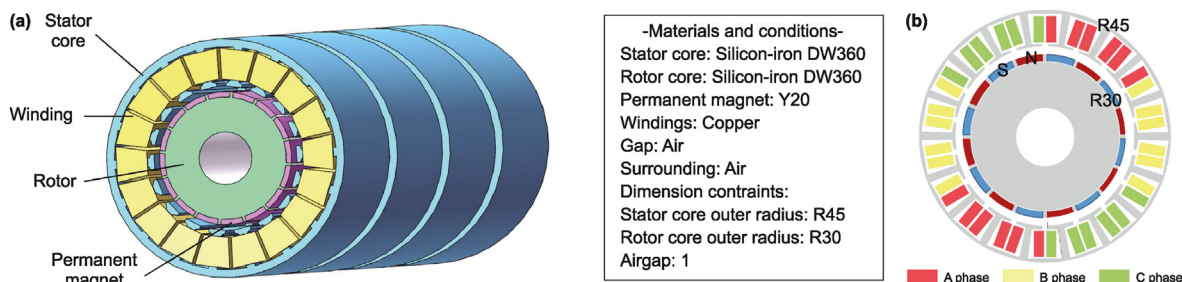


Fig. 2. Configuration of permanent magnet synchronous motor studied. (a) Three-dimensional model; (b) Design variables of the motor.

of PMSM obtained from Transient Structural module for one-way coupling methodology is imported into Maxwell module again in order to analyze the magnetic force for two-way coupling methodology. Moreover, the magnetic force calculated is imported into Transient Structural module again to compute the strain and torque on the motor shaft for two-way coupling methodology. And repeat the previous step until the relative error between the calculated torques is less than 1%.

Compared with two-way coupling methodology, these parameters such as the shaft strain and magnetic force of PMSM need not be imported into Maxwell module and Transient Structural module again and there are no subsequent iterative processes for one-way coupling methodology.

The three-phase current of PMSM stator winding (Korasli, 2008; Han et al., 2022) is expressed by Eq. (9).

$$\begin{cases} i_A = i_m \sin(2\pi ft + \theta) \\ i_B = i_m \sin(2\pi ft + \theta + 2\pi/3) \\ i_C = i_m \sin(2\pi ft + \theta - 2\pi/3) \end{cases} \quad (9)$$

where  $i_A$ ,  $i_B$  and  $i_C$  are the three-phase currents of the stator winding in A,  $i_m$  is the maximum value of the three-phase current in A,  $f$  is the frequency of the three-phase current in Hz,  $t$  is the working time of PMSM in s, and  $\theta$  is the initial phase angle of the current in rad.

Fig. 3 shows the electromagnetic torques of the PMSM with different motor spline clearances using the one-way and two-way coupling methodologies. And the calculated results of electromagnetic torque are compared with the measured ones. It is observed that the spline clearance of the motor is inversely proportional to the electromagnetic torque. When the spline clearance is increased from 150 to 350  $\mu\text{m}$ , the electromagnetic torque is dropped by about 10%. The average error between the simulated

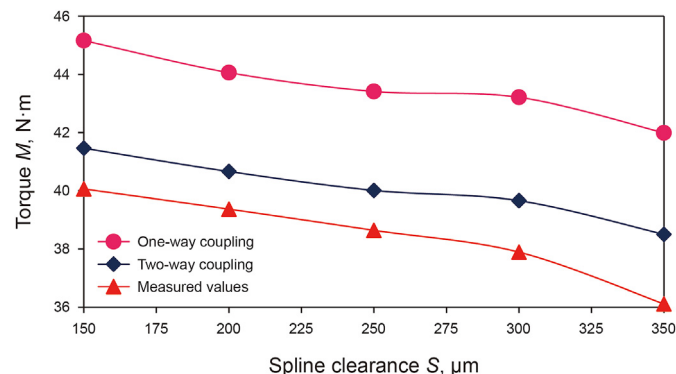


Fig. 3. Variation curves of motor electromagnetic torque with different spline clearances using the one-way and two-way coupling methodologies.

results and the measured results is 11.85%, while the electromagnetic torques of the PMSM are computed by the one-way coupling method. Furthermore, the average error between the simulated results and the measured results is only 4.13%, while we use the two-way coupling method proposed to analyze the electromagnetic torques. It can be concluded that the two-way coupling method provides a more accurate estimation of the electromagnetic torque than the one-way coupling method.

#### 4. Results and interpretation of model

##### 4.1. The influence of the spline clearance of the PMSM on the mechanical characteristics

To investigate the impact of spline clearance on the stress-strain behavior of the PMSM in electric submersible pumping wells, the stress-strain of the PMSM is analyzed using a two-way coupling method. There are many nodes that need to be processed and calculated at the spline teeth while meshing the three-dimensional solid model with the complicated multi-tooth structure. And it results in a large number of poor meshes generated and inaccurate finite element results. Consequently, the complex structure at the spline teeth has been simplified for the PMSM. And some unnecessary chamfers and shoulders have been removed from the spline connection of the 3D model (Fig. 1). These removed chamfers are composed of the edges of spline teeth and the boundary lines between each groove surface of spline grooves. These removed shoulders are mainly located at the joint between spline and motor shaft. The poly-hexcore mesh is used to achieve the electromagnetic torques with two-way magneto-mechanical coupling while this methodology can improve the predicted accuracies and save the calculated resources. The mesh has been refined near the tooth profiles of spline used in the PMSM.

The stress distribution of the NSR-PMSM and the SR-PMSM is shown in Fig. 4(a) and (b). The strain distribution of the NSR-PMSM and the SR-PMSM is shown in Fig. 5(a) and (b). It can be found from the figures that the maximum stress and strain appear adjacent to the surface of the spline joint. The problem of stress concentration in the spline joint is investigated under the aforementioned conditions.

The maximum stress-strain values of the PMSM at different spline clearances are shown in Table 2.

The increase in the spline clearance leads to the decrease in the maximum stress-strain of the SR-PMSM. When the spline clearance is increased from 150 to 350  $\mu\text{m}$ , the maximum stress is dropped by 5.86%, and the maximum strain is dropped by 5.89%. Consequently, the spline clearance at the spline joint changes the torsion angle of the rotor and reduces the electromagnetic forces applied to the rotor.

Fig. 6 shows the electromagnetic torque of the two types of motors at different spline clearances. The spline clearance ( $S$ ) is set

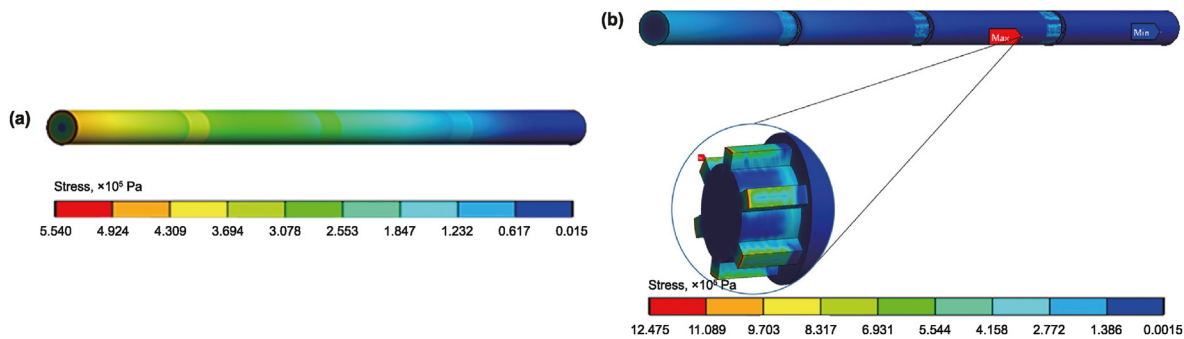


Fig. 4. Stress distribution of PMSM rotor. (a) NSR-PMSM; (b) SR-PMSM.

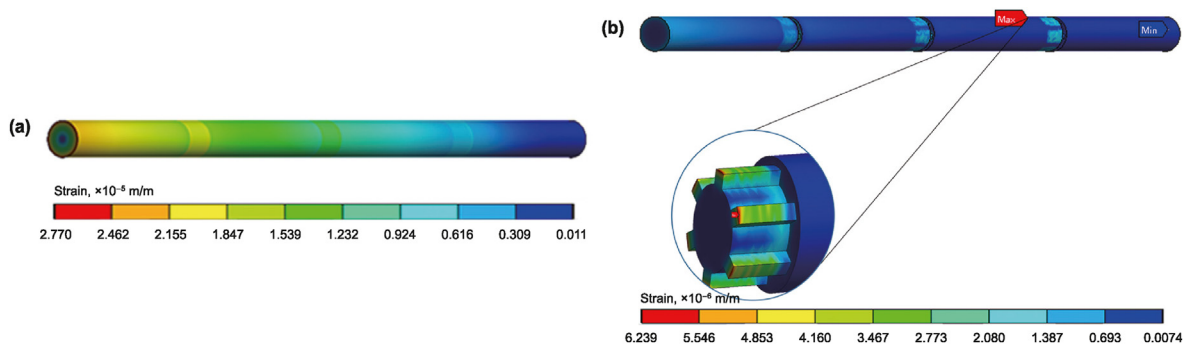


Fig. 5. Strain distribution of PMSM rotor. (a) NSR-PMSM; (b) SR-PMSM.

Table 2  
The maximum stress-strain of NSR-PMSM and SR-PMSM.

Rotor configurations	Spline clearance, $\mu\text{m}$	Maximum stress, Pa	Maximum strain, $\text{m} \cdot \text{m}^{-1}$
NSR-PMSM	0	$5.5396 \times 10^5$	$2.7699 \times 10^{-5}$
SR-PMSM	150	$1.2825 \times 10^6$	$6.4158 \times 10^{-6}$
	200	$1.2670 \times 10^6$	$6.3372 \times 10^{-6}$
	250	$1.2475 \times 10^6$	$6.2394 \times 10^{-6}$
	300	$1.2276 \times 10^6$	$6.1407 \times 10^{-6}$
	350	$1.2073 \times 10^6$	$6.0381 \times 10^{-6}$

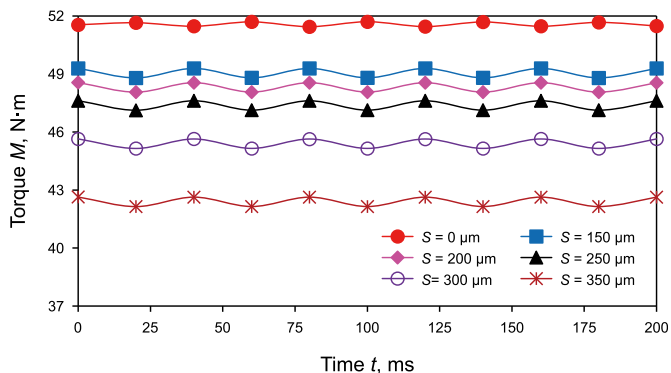


Fig. 6. Comparison of electromagnetic torque in NSR-PMSM and SR-PMSM with a change in spline clearances.

to 0  $\mu\text{m}$  for the NSR-PMSM. There is no need for spline connection between adjacent segment rotors of the NSR-PMSM. Therefore, a spline clearance of 0  $\mu\text{m}$  represents that the PMSM is not segmented (NSR-PMSM). The other five curves show the variations of the electromagnetic torque vs. time under different spline

clearances for the SR-PMSM. And the spline clearances ( $S$ ) of the SR-PMSM are set from 150 to 350  $\mu\text{m}$ . For the same conditions, the NSR-PMSM rotor produces a significantly higher electromagnetic torque than the SR-PMSM rotor.

The decline rate of the electromagnetic torque refers to the percentage of electromagnetic torque drop on the SR-PMSM rotor compared with the NSR-PMSM rotor. And it indicates the influence of spline clearance on the electromagnetic torque of PMSM. The decline rate of the electromagnetic torque at 150 rpm and a varying spline clearance is shown in Fig. 7.

The decline rate of the electromagnetic torque exhibits a relatively low value of 4.91% at a spline clearance of 150  $\mu\text{m}$ . When the spline clearance is 350 rpm, the decline rate of the electromagnetic torque increases to 17.82%. This result confirms that the decline rate of the electromagnetic torque is inversely proportional to the spline clearance.

#### 4.2. Comparison of electromagnetic torque according to operating conditions

The range of the rotation speed for the PMSM driving the submersible screw pump in this study is 150–400 rpm. The electromagnetic torque in the two PMSMs at different motor speeds using

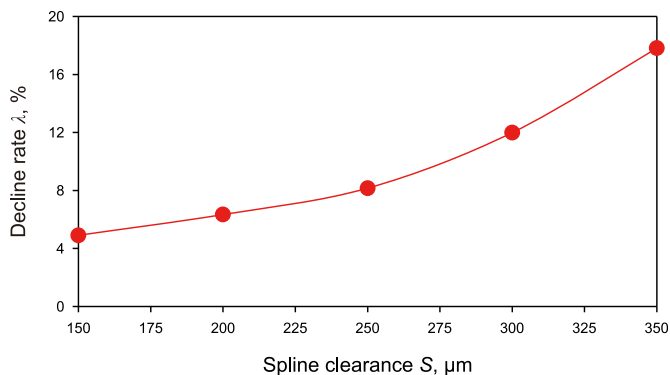


Fig. 7. Decline rate of the electromagnetic torque at different spline clearances.

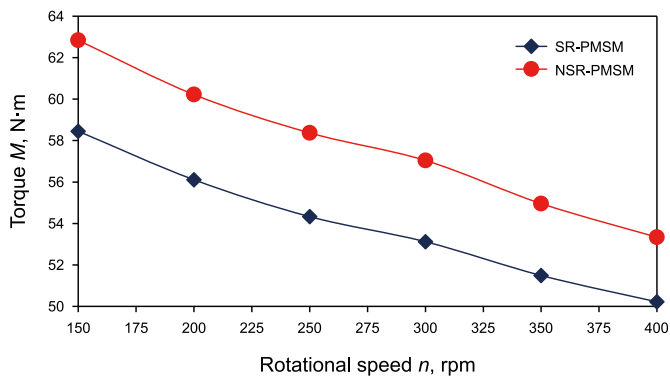


Fig. 8. Variation curves of the motor electromagnetic torque in NSR-PMSM and SR-PMSM under different rotational speed conditions.

the finite element method is obtained and compared in Fig. 8. The PMSM is controlled by magnetic field orientation vector. The stator currents are adjusted by the motor power device. And the magnetic field positions of the motor rotor are measured by sensors such as encoders. A certain relative position is maintained between the magnetic fields of the stator and the rotor in order to realize the precise control of the PMSM in electric submersible pumping wells.

With the increase in the motor's rotational speed, the electromagnetic torque of the PMSM decreases slightly. At a motor rotational speed of 400 rpm, the electromagnetic torques of the NSR-PMSM and the SR-PMSM are 53.34 and 50.22 N·m, respectively. Compared with the NSR-PMSM, this represents a decrease of 5.85% in the electromagnetic torque for the SR-PMSM. It can be found that the variations of electromagnetic torque reduction due to the existence of rotational speed are basically the same for the SR-PMSM and NSR-PMSM. But the NSR-PMSM exhibits a higher electromagnetic torque than the SR-PMSM under different rotational speed conditions. The main reason is that the effect of spline clearance on the electromagnetic torque of the SR-PMSM and NSR-PMSM does not vary with different rotational speeds, while it can be influenced by the motor residual magnetism and the magnetic field of permanent magnet and stator coil.

PMSMs are commonly used in oil wells over several kilometers deep (Huang et al., 2016; Zhang et al., 2017; Jia et al., 2021), where the ambient temperature is high and heat dissipation is poor (Clegg et al., 1990; Leupold and Potenziani, 1993; Moosavi et al., 2015). In this study, we analyze the electromagnetic torque of a PMSM under high-temperature conditions using finite element methods. Fig. 9 presents the electromagnetic torque of the two types of motors at

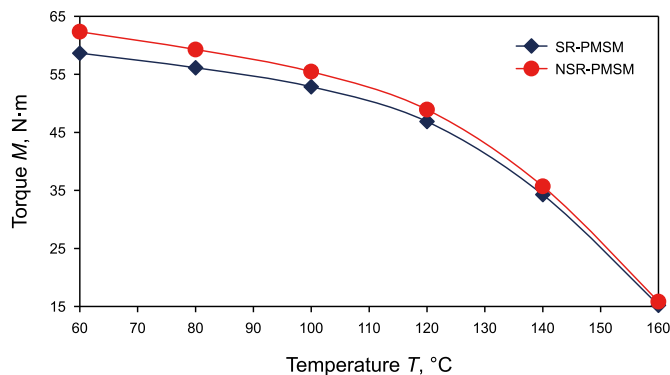


Fig. 9. Variation curves of the motor electromagnetic torque in the NSR-PMSM and SR-PMSM under different temperature conditions.

different temperature conditions. Generally, electromagnetic torque decreases with increasing temperature at any particular motor rotational speed, but the decrease is substantially higher at high temperatures than at low temperatures, in the temperature range considered. When the motor rotational speed is approximately 150 rpm with a temperature of 60 °C, the electromagnetic torques of NSR-PMSM and SR-PMSM are 62.34 and 58.66 N·m, respectively. This indicates a decrease of 5.9% in the electromagnetic torque of the SR-PMSM compared to the NSR-PMSM under high-temperature conditions.

Compared with the SR-PMSM, the variation of electromagnetic torque reduction due to the existence of temperature under high-temperature conditions is much higher than that in low-temperature conditions for the NSR-PMSM. The main reason is that the permanent magnet will gradually demagnetize under high-temperature conditions, which results in the weakening of the magnetic field strength of motor rotor. Moreover, the stator coil is made of copper, and the conductivity of copper under high-temperature conditions is slightly lower than that under low-temperature conditions, which weakens the magnetic field strength of motor stator and reduces the electromagnetic torque of the PMSM. In addition, the high ambient temperatures will also affect the viscosity of lubricating oil between stator and rotor and the shaft strain of each part of the PMSM, and these parameters will also have a small impact on the reduction of electromagnetic torque.

The decline rate of the electromagnetic torque serves as an indicator of the impact of spline clearance on the mechanical performance of the PMSM. A higher decline rate of the electromagnetic torque indicates the stronger effect of the spline clearance on the electromagnetic torque. Fig. 10 shows the decline rate of the electromagnetic torque at different operating conditions.

It is observed that the increase in the motor's rotational speed does not lead to changes in the decline rate of the electromagnetic torque. However, the increase in the ambient temperature results in a decrease in the decline rate of the electromagnetic torque. The maximum decline rate of the electromagnetic torque by the SR-PMSM at 400 rpm with a temperature of 60 °C is 7.04%. However, the presentation of the minimum decline rate of the electromagnetic torque is at a value of 3.92% when the motor rotational speed is approximately 150 rpm with a temperature of 160 °C. It can be concluded that there is no relationship between the influence of the spline clearance on the motor output performance and motor rotational speed, and the decline rate of the electromagnetic torque is inversely proportional to the temperatures.

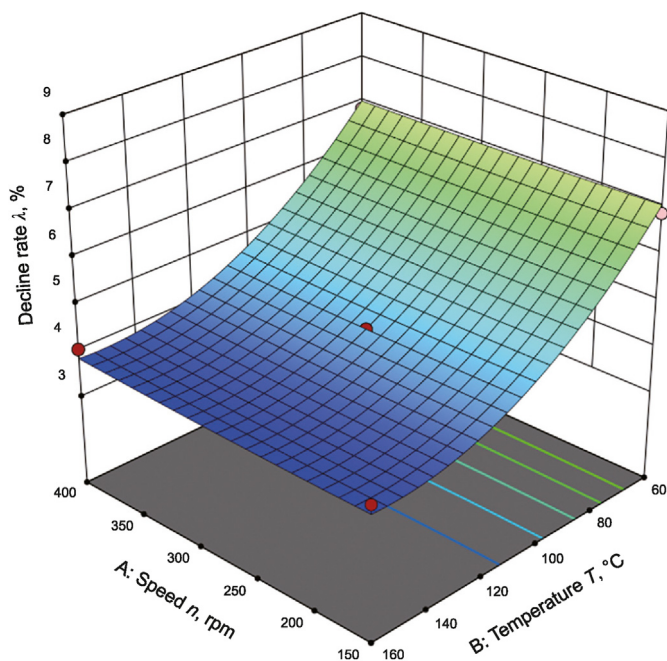


Fig. 10. Relationship between working conditions and electromagnetic torque.

### 5. The experimental results and interpretation

As shown in Fig. 11, a test platform was developed and experiments were carried out to reveal the effect of the spline clearance on the mechanical characteristics of PMSM. Fig. 11(a) illustrates the spline of motor shaft applied in the experimental prototype PMSM. The splines are used to connect adjacent motor shafts of segmented rotors in a PMSM-driven rodless lifting system. The variations of the decreased electromagnetic torque caused by the existence of spline clearance are almost the same between the 18-slot and 16-pole PMSM and the 12-slot and 10-pole PMSM. Moreover, the 12-slot and 10-pole PMSM has been processed and manufactured, and used as a prototype in the experiment. Consequently, the 12 slots and 10 poles are tested to verify the accuracy and the impact of the spline clearance on electromagnetic torque of 18-slot and 16-pole PMSM. And a 12-slot and 10-pole PMSM is used in the

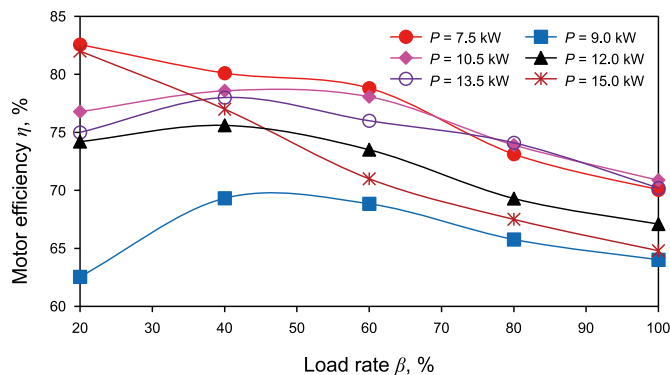


Fig. 12. Variation curves of the motor load characteristics at different powers.

experiment and the rated voltage and the power are 380 V and 7.5 kW, respectively (Fig. 11(b)). The output torque of the PMSM motor is measured using a torque transducer installed on the motor's rotor.

The variation curves of the load characteristics at different powers of the PMSM are presented in Fig. 12. It can be observed that the motor efficiencies are obviously low for the low-speed (150–400 rpm) PMSMs. And the losses caused by segmented rotors, centralizer bearings at the joints and thrust bearings at each shaft end increase under high temperature conditions. The motor efficiency of the PMSM whose power is 15 kW drops faster, which is caused by an increase in the number of segmented rotors of the motor and the total length of the motor. When the output rotational speed of the motor is constant, the number of segmented rotors of the motor is proportional to the motor losses, and the motor efficiency is higher than 60% for the load factors in the range of 20%–100%. This result indicates that the prototype of the PMSM meets the industrial operational requirements.

The various internal splines with different specifications are manufactured on the motor shafts, resulting in different clearance fits and spline clearances. And the output torque of the prototype is tested at different spline clearances to verify the impact of the spline clearance on the output performance of the PMSM. Fig. 13 presents the variation curves of the electromagnetic torque at different spline clearances.

The effect of the spline clearance on the electromagnetic torque

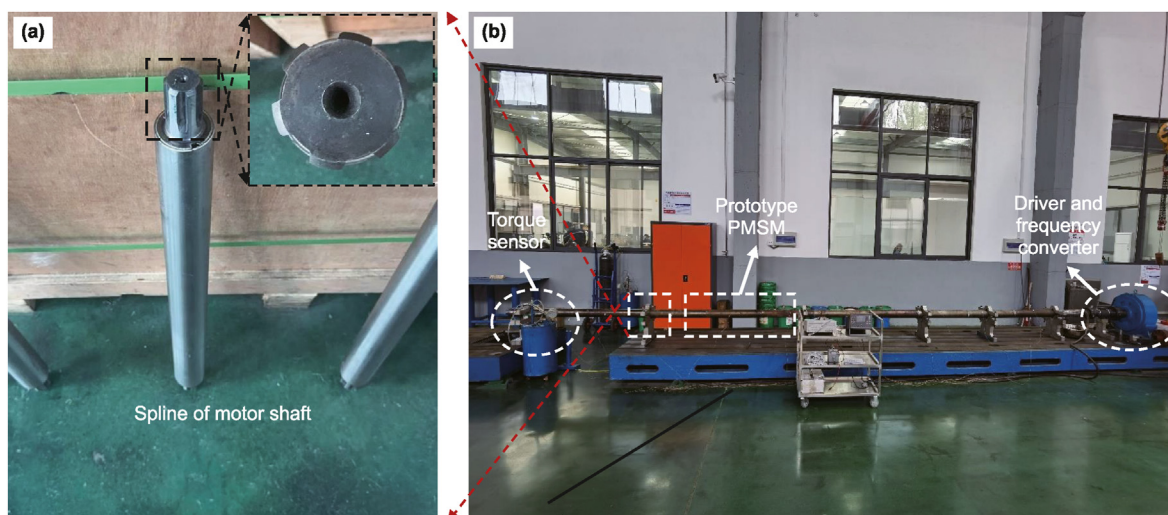


Fig. 11. A test platform of PMSM and its experimental prototype. (a) Spline of motor shaft; (b) Prototype PMSM, driver, converter and sensor of test platform.

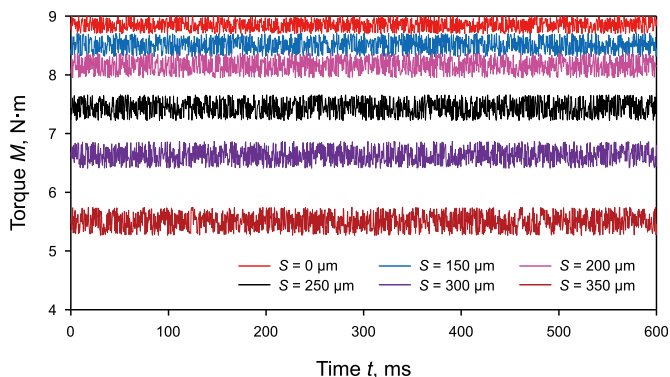


Fig. 13. Experimental results of electromagnetic torque of PMSM at different spline clearances.

is analyzed using the electromagnetic torque model and finite element analysis. The patterns of variation of electromagnetic torque reduction due to the existence of spline gap are basically the same for 18-slot and 16-pole PMSMs and 12-slot and 10-pole PMSMs. The main reason is that the prototype PMSMs with 18-slot and 16-pole and 12-slot and 10-pole used in the experiment and finite element analysis are manufactured and made of multiple segment rotors and have the same basic structure. And there is a clearance fit between adjacent segment rotors. The spline clearance of the motor is inversely proportional to the electromagnetic torque. The shaft strain of PMSM enhances and the angle of magnetic field between stator and rotor reduces with the increase in the spline clearance, which leads to the faster decline of electromagnetic torque on the motor shaft.

Moreover, the electromagnetic torque of 12-slot and 10-pole PMSM decreases faster than that of 18-slot and 16-pole PMSM with the increased spline clearance. The main reason is that 18-slot and 16-pole PMSM used in finite element analysis is composed of four segment rotors in order to ensure the quality of the grid, while 12-slot and 10-pole PMSM used in the experiment is made of more segment rotors. The spline clearance in the front part leads to the rotation of the motor shaft, which will affect the angles between adjacent segment rotors. More segment rotors make the PMSM more susceptible to the spline clearance.

The experimental and theoretical results of the electromagnetic torque obtained from the electromagnetic torque model and measurement are shown in Fig. 14.

The measured electromagnetic torque of the PMSM are compared with the finite element analysis results. It can be seen

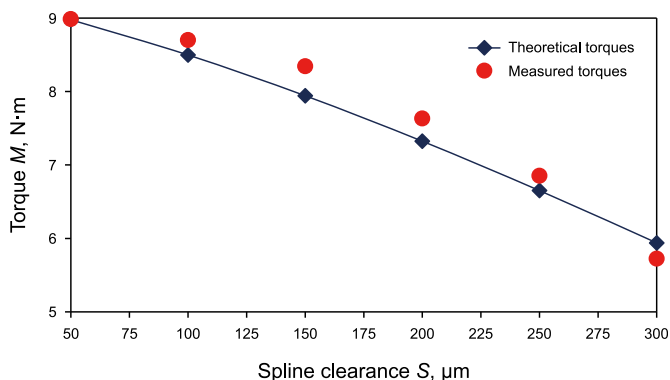


Fig. 14. Comparison of measured results and theoretical results of electromagnetic torque.

from the figure that the finite element analysis results agree well with the measured results. The maximum relative error between the finite element analysis and measured results for the SR-PMSM is approximately 4.82%. The result demonstrates that the mathematical model of electromagnetic torque is accurate.

## 6. Conclusions

The electromagnetic characteristics of PMSM with segmented rotors were comprehensively investigated and compared with a PMSM with non-segmented rotors through the two-way magneto-mechanical coupling method and experimental verification. The simulation results of the electromagnetic torque were compared under different working conditions to analyze the effect of spline clearances with different motors on electromagnetic torque. Finally, a test platform of PMSM was developed and a series of tests were performed to verify the accuracy of calculation and simulation.

The electromagnetic torques of NSR-PMSM and SR-PMSM were calculated under different conditions and compared with the measured results. The maximum errors between the simulation and the measured torques in SR-PMSM are 11.85% and 4.13% using the one-way coupling method and the two-way coupling method, respectively. The electromagnetic torque of the PMSM is inversely proportional to the spline clearance based on the simulation and experimental results. The experimental results obtained from the prototype agree well with the theoretical results using the two-way coupling method proposed.

The maximum stress-strain of the SR-PMSM is inversely proportional to the spline clearance with the varied position of the permanent magnets. The decline rate of electromagnetic torque is proportional to spline clearance, and the presence of spline clearance can lead to performance degradation in PMSMs. And the decline rate does not enhance significantly with the output speed, while it decreases with increasing temperature at some particular rotational speed. Then the mechanical properties of PMSMs in electric submersible pumping wells are more strongly influenced by the spline clearance as the ambient temperature is constantly rising.

## CRedit authorship contribution statement

**Xin-Fu Liu:** Writing – original draft, Software, Project administration, Funding acquisition. **Chun-Hua Liu:** Writing – review & editing, Resources, Methodology, Funding acquisition. **Ying Zheng:** Project administration, Methodology. **Ji-Fei Yu:** Resources, Project administration, Funding acquisition. **Wei Zhou:** Validation, Project administration, Funding acquisition. **Meng-Xiao Wang:** Supervision, Formal analysis, Data curation. **Peng Liu:** Resources, Methodology. **Yi-Fei Zhou:** Software, Data curation.

## Declaration of competing interest

No potential conflict of interest was reported by the authors.

## Acknowledgements

This work was financially supported by National Natural Science Foundation of China (Grant Nos. 52074161 and 52005281), Taishan Scholar Project of Shandong Province (Grant No. tsqn202211177), Shandong Provincial Plan for Introduction and Cultivation of Young Pioneers in Colleges and Universities (Grant No. 2021-Qing Chuang-30613019), Natural Science Foundation of Shandong Province (Grant Nos. ZR2022ME173 and ZR2023QE011) and Projects of CNOOC Research Institute Ltd. (Grant Nos.

CCL2023RCP0237RSN and CCL2023RCP0319RSN). The authors sincerely thanks to the anonymous reviewers for their insightful comments and suggestions. And the authors gratefully acknowledge the PetroChina technicians for their support, contributions and useful discussions.

## References

- Ahn, J.M., Son, J.C., Lim, D.K., 2021. Optimal design of outer-rotor surface mounted permanent magnet synchronous motor for cogging torque reduction using territory particle swarm optimization. *J. Electr. Eng. Technol.* 16, 429–436. <https://doi.org/10.1007/s42835-020-00599-z>.
- Ahmed, S., Toliyat, H.A., 2007. Coupled field analysis needs in the design of submersible electric motors. In: 2007 IEEE Electric Ship Technologies Symposium, pp. 231–237. <https://doi.org/10.1109/ESTS.2007.372091>.
- Akpan, U.O., Koko, T.S., Orisamolu, I.R., Gallant, B.K., 2001. Practical fuzzy finite element analysis of structures. *Finite Elem. Anal. Des.* 38 (2), 93–111. [https://doi.org/10.1016/S0168-874X\(01\)00052-X](https://doi.org/10.1016/S0168-874X(01)00052-X).
- Cortes, B., Araujo, L., Penido, D., 2019. Electrical submersible pump system model to assist oil lifting studies. *J. Petrol. Sci. Eng.* 174, 1279–1289. <https://doi.org/10.1016/j.petrol.2018.11.055>.
- Chen, P., Wang, D.H., Wang, B.D., Li, J.C., Xu, C., Wang, X.H., 2022. Torque ripple and electromagnetic vibration suppression in permanent magnet synchronous motor using segmented rotor with different pole widths. *IEEE T. Magn.* 58 (9), 1–5. <https://doi.org/10.1109/TMAG.2022.3179278>.
- Chen, S.J., Zhang, Q., He, B., Huang, S.R., Hui, D.D., 2017. Thermal analysis of high density permanent magnet synchronous motor based on multi physical domain coupling simulation. *J. Electr. Eng. Technol.* 12 (1), 91–99. <https://doi.org/10.5370/JEET.2017.12.1.091>.
- Clegg, A.G., Coulson, I.M., Hilton, G., Wong, H.Y., 1990. The temperature stability of NdFeB and NdFeBCo magnets. *IEEE T. Magn.* 26 (5), 1942–1944. <https://doi.org/10.1109/20.104578>.
- Cui, J.G., Xiao, W.S., Zou, W.Q., Liu, S.M., Liu, Q., 2020. Design optimization of submersible permanent magnet synchronous motor by combined DOE and taguchi approach. *IET Electr. Power Appl.* 14, 1060–1066. <https://doi.org/10.1049/iet-epa.2019.0346>.
- Ding, W., Hu, Y.F., Wang, T., Yang, S., 2017. Comprehensive research of modular E-Core stator hybrid-flux switched reluctance motors with segmented and non-segmented rotors. *IEEE Trans. Energy Convers.* 32 (1), 382–393. <https://doi.org/10.1109/TEC.2016.2631248>.
- Dong, Q.C., Liu, X.T., Qi, H.Z., Sun, C., Wang, Y.S., 2019. Analysis and evaluation of electromagnetic vibration and noise in permanent magnet synchronous motor with rotor step skewing. *Sci. China Technol. Sci.* 62, 839–848. <https://doi.org/10.1007/s11431-018-9458-5>.
- Duarte, F., Ferreira, A., Fael, P., 2018. Road pavement energy-harvesting device to convert vehicles' mechanical energy into electrical energy. *J. Energy Eng.* 144 (2), 04018003. [https://doi.org/10.1061/\(ASCE\)EY.1943-7897.0000512](https://doi.org/10.1061/(ASCE)EY.1943-7897.0000512).
- Fan, Z.M., Liu, G.W., Jin, S., Song, Z.H., Wang, J.Q., 2022. Comparative study on torque characteristics of permanent magnet synchronous reluctance motors with different axial hybrid rotors. *Energy Rep.* 36 (8), 1349–1359. <https://doi.org/10.1016/j.egy.2022.03.023>.
- Fang, M.Q., Raveendran, R., Huang, B., 2021. Real-time performance monitoring of electrical submersible pumps in SAGD process. *IFAC-PapersOnLine* 54 (11), 139–144. <https://doi.org/10.1016/j.ifacol.2021.10.064>.
- Freytag, M., Shapiro, V., Tsukanov, I., 2011. Finite element analysis in situ. *Finite Elem. Anal. Des.* 47 (9), 957–972. <https://doi.org/10.1016/j.finel.2011.03.001>.
- Gao, C.X., Gao, M.Z., Si, J.K., Hu, Y.H., Gan, C., 2019. A novel direct-drive permanent magnet synchronous motor with toroidal windings. *Energies* 12 (3), 432–438. <https://doi.org/10.3390/en12030432>.
- Ghoroghchian, F., Aliabad, A.D., Amiri, E., 2020. Design and analysis of consequent-pole line start permanent magnet synchronous motor. *IET Electr. Power Appl.* 14 (4), 678–684. <https://doi.org/10.1049/iet-epa.2019.0524>.
- Guemes, J.A., Iraolagoitia, A.M., DelHoyo, J.I., Fernandez, P., 2011. Torque analysis in permanent-magnet synchronous motors: a comparative study. *IEEE Trans. Energy Convers.* 26 (1), 55–63. <https://doi.org/10.1109/TEC.2010.2053374>.
- Han, T.H., Ko, S.C., Lim, S.H., 2022. Analysis on three-phase ground fault current limiting operations of three-phase transformer type SFCL using two superconducting modules. *IEEE Trans. Appl. Supercond.* 32 (6), 5601507. <https://doi.org/10.1109/TASC.2022.3181571>.
- Hao, Z.X., Zhu, S.J., Pei, X.H., Huang, P., Tong, Z., Wang, B.Y., Li, D.Y., 2019. Submersible direct-drive progressing cavity pump rodless lifting technology. *Petrol. Explor. Dev.* 46 (3), 621–628. [https://doi.org/10.1016/S1876-3804\(19\)60042-X](https://doi.org/10.1016/S1876-3804(19)60042-X).
- Hasanien, H.M., 2010. Torque ripple minimization of permanent magnet synchronous motor using digital observer controller. *Energy Convers. Manag.* 51 (1), 98–104. <https://doi.org/10.1016/j.enconman.2009.08.027>.
- Hong, J.M., Talbot, D., Kahraman, A., 2014. Load distribution analysis of clearance-fit spline joints using finite elements. *Mech. Mach. Theor.* 74, 42–57. <https://doi.org/10.1016/j.mechmachtheory.2013.11.007>.
- Huang, Z.Y., Fang, J.C., Liu, X.Q., Han, B.C., 2016. Loss calculation and thermal analysis of rotors supported by active magnetic bearings for high-speed permanent-magnet electrical machines. *IEEE Trans. Ind. Electron.* 63 (4), 2027–2035. <https://doi.org/10.1109/TIE.2015.2500188>.
- Ilka, R., Alinejad-Beromi, Y., Yaghobi, H., 2018. Cogging torque reduction of permanent magnet synchronous motor using multi-objective optimization. *Math. Comput. Simulat.* 153, 83–95. <https://doi.org/10.1016/j.matcom.2018.05.018>.
- Isildar, A., Van Hullebusch, E.D., Lenz, M.D., Laing, G., Marra, A., Cesaro, A., Panda, S., Akcil, A., Kucuker, M.A., Kuchta, K., 2019. Biotechnological strategies for the recovery of valuable and critical raw materials from waste electrical and electronic equipment (WEEE) - a review. *J. Hazard Mater.* 362, 467–481. <https://doi.org/10.1016/j.jhazmat.2018.08.050>.
- Iwashita, Y., Abe, M., Yako, T., Fuwa, Y., Terunuma, N., 2020. Bipolar correction magnet with permanent magnets. *IEEE Trans. Appl. Supercond.* 30 (4), 4003703. <https://doi.org/10.1109/TASC.2020.2968042>.
- Ji, H.C., 2008. Sequence stratigraphy and depositional systems in the paleogene, Liaodong Bay. *Petrol. Sci.* 5 (2), 110–118. <https://doi.org/10.1007/s12182-008-0018-0>.
- Jia, M.X., Hu, J.J., Xiao, F., Yang, Y., Deng, C.H., 2021. Modeling and analysis of electromagnetic field and temperature field of permanent-magnet synchronous motor for automobiles. *Electronics* 17 (10), 2173–2181. <https://doi.org/10.3390/electronics10172173>.
- Johnson, O.A., Affam, A.C., 2019. Petroleum sludge treatment and disposal: a review. *Environ. Eng. Res.* 24 (2), 191–201. <https://doi.org/10.4491/eeer.2018.134>.
- Khulief, Y.A., Al-Naser, H., 2005. Finite element dynamic analysis of drillstrings. *Finite Elem. Anal. Des.* 41 (13), 1270–1288. <https://doi.org/10.1016/j.finel.2005.02.003>.
- Kim, H.S., 2001. Finite element analysis of torsional deformation. *Mat. Sci. Eng. A - Struct.* 299 (1–2), 305–308. [https://doi.org/10.1016/S0921-5093\(00\)01416-7](https://doi.org/10.1016/S0921-5093(00)01416-7).
- Kim, S.I., Lee, J.Y., Kim, Y.K., Hong, J.P., Hur, Y., Jung, Y.H., 2005. Optimization for reduction of torque ripple in interior permanent magnet motor by using the taguchi method. *IEEE T. Magn.* 41 (5), 1796–1799. <https://doi.org/10.1109/TMAG.2005.846478>.
- Klemz, A.C., Weschenfelder, S.E., Neto, S.L.C., Damas, M.S.P., Viviani, J.C.T., Mazur, L.P., Marinho, B.A., Pereira, L.S., Da-Silva, A., Valle, J.A.B., 2021. Oilfield produced water treatment by liquid-liquid extraction: a review. *J. Petrol. Sci. Eng.* 199, 108282. <https://doi.org/10.1016/j.petrol.2020.108282>.
- Korasli, C., 2008. Three-phase current measurement using single toroidal-core current transformer. *Elec. Power Compon. Syst.* 36 (3), 213–223. <https://doi.org/10.1080/15325000701603769>.
- Leupold, H.A., Potenziari, E., 1993. Choice of material in the design of permanent magnet flux sources. *IEEE T. Magn.* 29 (6), 3016–3018. <https://doi.org/10.1109/20.281105>.
- Li, Z., He, W., Liu, L.Q., Wang, Q.J., 2019. Magnetic field calculation and dynamics simulation of a permanent magnetic hybrid driven 3-DOF motor. *J. Electr. Eng. Technol.* 14 (2), 711–718. <https://doi.org/10.1007/s42835-018-00064-y>.
- Lim, D.K., Jung, S.Y., Jung, H.K., Ro, J.S., 2017. Analytical prediction of cogging torque for interior permanent magnet synchronous motors. *Int. J. Appl. Electromagn. Mech.* 55 (4), 625–635. <https://doi.org/10.3233/JAE-170094>.
- Liu, X.F., Liu, C.H., Hao, Z.X., Zheng, Y., Zhang, K., Wang, J.F., Wei, S.B., Hao, A.G., Tao, J.L., Cheng, H., 2023. Non-symmetric distributions of solids deposition for solid-water stratified flow in deviated tubing strings. *Petrol. Sci.* 20 (5), 3048–3061. <https://doi.org/10.1016/j.petsci.2023.03.017>.
- Liu, Z., Hu, Y., Wu, J.C., Zhang, B.Y., Feng, G.H., 2021. A novel modular permanent magnet-assisted synchronous reluctance motor. *IEEE Access* 152 (9), 19947–19959. <https://doi.org/10.1109/ACCESS.2021.3054766>.
- Moosavi, S.S., Djerdir, A., Amirat, Y.A., Khaburi, D.A., 2015. Demagnetization fault diagnosis in permanent magnet synchronous motors. *J. Magn. Magn. Mater.* 391, 203–212. <https://doi.org/10.1016/j.jmmm.2015.04.062>.
- Morimoto, E., Hirata, K., Niguchi, N., Ohno, Y., 2014. Design and analysis of magnetic-gear motor with field windings. *IEEE T. Magn.* 50 (11), 8204204. <https://doi.org/10.1109/TMAG.2014.2320526>.
- Morimoto, S., Sanada, M., Takeda, Y., 2001. Performance of PM-assisted synchronous reluctance motor for high-efficiency and wide constant-power operation. *IEEE Trans. Ind. Appl.* 37 (5), 1234–1240. <https://doi.org/10.1109/28.952497>.
- Nishino, A., Ueda, K., Fujii, K., 2017. Design of a new torque standard machine based on a torque generation method using electromagnetic force. *Meas. Sci. Technol.* 28 (2), 025005. <https://doi.org/10.1088/1361-6501/28/2/025005>.
- Qiao, Z.W., Shi, T.N., Wang, Y.D., Yan, Y., Xia, C.L., He, X.N., 2013. New sliding-mode observer for position sensorless control of permanent-magnet synchronous motor. *IEEE Trans. Ind. Electron.* 60 (2), 710–719. <https://doi.org/10.1109/TIE.2012.2206359>.
- Rallabandi, V., Fernandes, B.G., 2014. Design procedure of segmented rotor switched reluctance motor for direct drive applications. *IET Electr. Power Appl.* 8 (3), 77–88. <https://doi.org/10.1049/iet-epa.2013.0154>.
- Redinz, J.A., 2023. Magnetic energy in quasistatic systems. *Eur. J. Phys.* 44 (1), 015202. <https://doi.org/10.1088/1361-6404/ac9ba5>.
- Singhal, S., Singh, K.V., Hyder, A., 2011. Effect of laminated core on rotor mode shape of large high speed induction motor. In: 2011 IEEE International Electric Machines & Drives Conference (IEMDC), pp. 1557–1562. <https://doi.org/10.1109/IEMDC.2011.5994842>.
- Spalek, D., 2010. Anisotropy component of electromagnetic force and torque. *B. Pol. Acad. Sci. - Tech.* 58 (1), 107–117. <https://doi.org/10.2478/v10175-010-0011-9>.
- Wan, Z.P., Sun, B., Wang, X.W., Wen, W.Y., Tang, Y., 2020. Improvement on the heat dissipation of permanent magnet synchronous motor using heat pipe. *P. I. Mech. Eng. D- J. Aut.* 234 (5), 1249–1259. <https://doi.org/10.1177/0954407019880444>.
- Wang, C.Y., Xia, J.K., Shun, Y.B., 2009. *Modern Motor Control Technology*. China Machine Press, China, Beijing.

- Wang, J., Qu, R.H., Zhou, L.B., 2012. Dual-rotor multiphase permanent magnet machine with harmonic injection to enhance torque density. *IEEE Trans. Appl. Supercond.* 22 (3), 5202204. <https://doi.org/10.1109/TASC.2011.2179399>.
- Wang, S.C., Nien, Y.C., Huang, S.M., 2022. Multi-objective optimization design and analysis of V-shape permanent magnet synchronous motor. *Energies* 15 (10), 3496. <https://doi.org/10.3390/en15103496>.
- Xu, W., Xu, J., Zhang, W.H., Wang, J.Y., 2023. A combined-pole permanent magnet synchronous motor incorporating nanocomposite magnets. *J. Magn. Magn. Mater.* 577, 170807. <https://doi.org/10.1016/j.jmmm.2023.170807>.
- Yang, Z., Zhang, H.L., 2008. Strategies for development of clean energy in China. *Petrol. Sci.* 5 (2), 183–188. <https://doi.org/10.1007/s12182-008-0029-x>.
- Yang, Z.G., Li, W., Gou, Y.N., Cai, T.F., 2020. Research on radial force of permanent magnet synchronous motor based on maxwell. *J. Electr. Eng. Technol.* 15 (3), 2601–2608. <https://doi.org/10.1007/s42835-020-00511-9>.
- Zhang, G., Hua, W., Cheng, M., Zhang, B.F., Guo, X.B., 2017. Coupled magnetic-thermal fields analysis of water cooling flux-switching permanent magnet motors by an axially segmented model. *IEEE T. Magn.* 53 (6), 351–354. <https://doi.org/10.1109/TMAG.2017.2668845>.
- Zhang, W.J., Huang, S.D., Gao, J., Li, R., Dai, L.T., 2018. Electromagnetic torque analysis for all-harmonic-torque permanent magnet synchronous motor. *IEEE T. Magn.* 54 (11), 1–5. <https://doi.org/10.1109/TMAG.2018.2839032>.
- Zhang, B.Y., Liang, B.X., Feng, G.H., Zhuang, F.Y., 2007. Research of multipolar permanent magnet synchronous submersible motor for screw pump. In: 2007 International Conference on Mechatronics and Automation, pp. 1011–1016. <https://doi.org/10.1109/ICMA.2007.4303686>.
- Zhang, Y.H., Yang, K., 2022. Fault diagnosis of submersible motor on offshore platform based on multi-signal fusion. *Energies* 15 (3), 756–766. <https://doi.org/10.3390/en15030756>.
- Zhao, J., Wang, Z.B., Liu, H.Q., Ning, F., Hong, X.W., Du, J.J., Yu, M., 2020. Modal analysis and structure optimization of permanent magnet synchronous motor. *IEEE Access* 151 (8), 151856–151865. <https://doi.org/10.1109/ACCESS.2020.3017679>.
- Zhu, Y.R., Zhang, J.J., Li, H.Y., Chen, J., 2007. Characteristic temperatures of waxy crude oils. *Petrol. Sci.* 4 (3), 57–62. <https://doi.org/10.1007/s12182-007-0010-0>.